Distribution of Large Biomass Particles in a Sand-Biomass Fluidized Bed: Experiments and Modeling

Farzam Fotovat and Jamal Chaouki
Dept. of Chemical Engineering, École Polytechnique de Montréal, C.P. 6079 succ., Centre Ville, Montreal, QC H3C 3A7, Canada

Jeffrey Bergthorson
Dept. of Mechanical Engineering, McGill University, Macdonald Engineering Building, 817 Sherbrooke Street West, Montreal, QC H3A 2K6, Canada

DOI 10.1002/aic.14337
Published online January 16, 2014 in Wiley Online Library (wileyonlinelibrary.com)

The axial distribution of large biomass particles in bubbling fluidized beds comprised of sand and biomass is investigated in this study. The global and local pressure drop profiles are analyzed in mixtures fluidized at superficial gas velocities ranging from 0.2 to 1 m/s. In addition, the radioactive particle tracking technique is used to track the trajectory of a tracer mimicking the behavior of biomass particles in systems consisting of 2, 8, and 16% of biomass mass ratio. The effects of superficial gas velocity and the mixture composition on the mixing/segregation of the bed components are explored by analyzing the circulatory motion of the active tracer. Contrary to low fluidization velocity ($U = 0.36$ m/s), biomass circulation and distribution are enhanced at $U = 0.64$ m/s with increasing the load of biomass particles. The axial profile of volume fraction of biomass along the bed is modeled on the basis of the experimental findings. © 2014 American Institute of Chemical Engineers *AIChE J*, 60: 869–880, 2014
Keywords: fluidization, mixing, biomass, particle tracking, pressure analysis

Introduction

Producing energy from biomass provides a key substitution for fossil fuel sources which results in the mitigation of greenhouse gas emissions. Additionally, use of biomass in forms of municipal and agricultural waste as an energy resource relieves the problem of waste management in favor of developing localized plants of energy production.

Thermochemical and biochemical processes are known as the most widespread technologies to convert biomass into energy or value-added synthetic fuels. The main processes used within the thermochemical conversion process are the following: combustion, pyrolysis, gasification, and liquefaction. Several unique operational advantages, like fuel flexibility, intense solids mixing, and efficient heat transfer, have made the fluidized bed the most efficient reactor for all of these processes. Nonetheless, fluidization of biomass particles is a cumbersome or even impossible task owing to their irregular size, density, and shape. Generally, an inert material, like silica sand, alumina, calcite and so forth, is added to biomass to assist its fluidization and improve the heat transfer; however, some new multiphase flow complexities arise as a consequence of the fluidization of dissimilar components. Understanding and managing multiphase flows are critical for the successful design of biomass conversion units and for improving the existing biomass processes.[1] One of the most undesirable multiphase flow phenomena in fluidization units comprising dissimilar components is the tendency of particles to be segregated along the bed. In general, particles which are larger in size or higher in density, tend to sink to the bottom of the bed (jetsam particles), whereas those that are smaller in size or lower in density move up to the bed surface (flotsam particles). Possessing very low densities, biomass particles behave regularly like flotsam in mixtures composed of sand and biomass and are likely to accumulate at the top of the bed.

The mass content of fuel, for example, coal or biomass, as a percentage of the total bed mass in bubbling bed combustion or gasification conditions is typically about 1–5%, depending on the fuel type, size, and reactivity. Considering the relatively low fraction of biomass in the mixture, the impact of biomass particles on the hydrodynamic characteristics of the fluidization medium has generally been neglected. Assuming insignificant interaction between multiple large objects, the common approach to study the motion of fuel particles in fluidization conditions is immersing a single large/light object in a bed of relatively small/dense particles.[2–4]

Fuel particles are subject to thermal fragmentation as they are fed into the reactor. However, it can be shown that the time needed to reach the bed temperature increases dramatically with the size of fuel particles. For instance, on the basis of the energy balance for a single particle, a 10-mm wood particle, which is comparable to the materials used in the present study, takes tens of seconds to reach 800°C under bubbling fluidization conditions.[5] During this considerable

Correspondence concerning this article should be addressed to J. Chaouki at jamal.chaouki@polymtl.ca.

period of time, the mixing/segregation pattern of the bed can fully be established.

A few researchers have deployed particle tracking techniques to study the motion and mixing mechanisms of the objects possessing a larger size and lower density than the bed material. Using cinematographic recording and a radioactive tracer, Rios et al.[6] investigated the characteristic motions and the velocity of such particles as a function of superficial gas velocity, characteristics of bed material, and bed height in two-dimensional (2-D) and three-dimensional columns. Lim and Agarwal[7] utilized the automated image analysis methods to characterize the circulation pattern and measure the velocity of a light sphere 7 mm in diameter immersed in a 2-D bubbling fluidized bed of 0.7-mm glass ballotini. Pallares and Johnsson[8] tracked phosphorescent tracers varying in size and density in a 2-D riser to obtain the concentration, velocity, and dispersion field of the fuel-like particles. Using digital image analysis in a 2-D bubbling fluidized bed, Soria-Verdugo et al.[2,3] studied circulation of a large cylindrical object with the same density of the bed material and explored the effect of buoyant forces on the motion of objects with different sizes and densities.

Use of the radioactive particle tracking (RPT) technique for studying the solid circulation patterns in binary mixtures was initially introduced by Larachi et al.[9] Cassanello et al.[10] adopted this technique to investigate solids mixing in gas–liquid–solid fluidized beds. More recently, Upadhyay and Roy[11] used this method to explore the mixing and hydrodynamic behavior in a bed consisting of equal weight percentages of the same size particles differing in density.

Zhang et al.[12] studied the effect of biomass ratio on the fluidization behavior of mixtures composed of 1–3% biomass. They found that the composition of mixtures had a quantitative impact on the ultimate distribution of biomass particles, that is, increasing the ratio of biomass to sand at $U > U_{ff}$ led to the occurrence of a greater maximum of mixing index at higher gas velocities. They have also reported that when mixing prevailed against segregation, increasing the biomass load exerted an adverse influence on the mixing; in contrast, as the increase of gas velocity enhanced particle segregation, increasing biomass load improved particle mixing.[13]

Despite the widespread application for fluidization of a bulk of large and light Geldart D particles[14] mixed with a fluidization medium of Geldart B, the phenomenological knowledge about their mixing pattern is still scarce. Accordingly, this work is aimed at deploying the powerful, nonintrusive RPT technique to shed some light on the distribution profile and circulatory motion of biomass particles fluidized with the help of sand. Moreover, the experimental findings have been used to develop a model predicting the volume concentration of biomass along the bed.

Indeed, the density of biomass particles decreases during their pyrolysis and segregation is enhanced. As the density of the tracer used in this study was constant during the experiment, such a phenomenon could not be mimicked. However, this phenomenon can be addressed in the RPT experiments by using a tracer with lower density compared to the conventional biomass materials. Moreover, gas properties, such as density and viscosity, are different in a cold system from those of a hot system where gas has much lower density and higher viscosity. These differences should be taken into consideration before applying the results of this work to the practical units operating at extreme conditions.

It should be noted that as the fluidization of binary systems consisting of common bed materials and irregular particles is not limited to biomass processing, the range of weight fractions investigated in the present study extends beyond the typical maximum biomass loads in industrial units.

Experimental

A cylindrical Plexiglas column 152 mm in diameter is used as the main facility of all experiments performed in the present study. Air is injected into the column through 163 holes, 1 mm in diameter, arranged in a triangular pitch on a stainless steel distributor plate. The percentage of open area of the perforated plate is less than 1. It is worth pointing out that the cross section of the commercial biomass combustors or gasifiers may be as large as a few square meters, while the column diameter used in this study is quite limited. Such a small column diameter may affect motion and mixing of the bed inventory particles.

The bed material utilized in the experiments is sand whose size distribution ranges from 100 to 1000 μm. As only one tracer can be tracked in the RPT technique, no variety of size and shape of biomass particles could be considered in the experiments and identical biomass particles are used in the system represented well by an active tracer. Accordingly, wood rods are carefully cut into similar cylindrical pieces to make identical biomass particles.

It should be kept in mind that in reality, a broad range of biomass particles, in terms of size and shape, is fed into the thermal processing unit complicating the hydrodynamic and reaction phenomena. Moreover, biomass degrades into fine char (in pyrolysis and gasification) or ash (in combustion) particles and its proportion and properties change with location in the bed. These deviations from the practical systems have not been addressed in this work. Nonetheless, as mentioned earlier, large biomass particles remain for a relatively long period of time at their original size before they reach the high temperatures which is needed for thermal degradation. This period is long enough for forming the distribution pattern of particles in the bed.

Properties of materials used in the present study have been listed in Table 1. Measured quantities of these materials are mixed to obtain the desired weight fraction of the biomass in the mixture. Table 2 contains more details of the mixtures studied.

In all experiments, the static bed height is set to 228 mm ($H/D = 1.5$).To start from a well-mixed condition, the sand and biomass measures are each equally divided into eight batches. Each batch of sand is mixed with a single batch of biomass. Finally, the content of all mixtures is added sequentially to the fluidization column.

Two differential pressure transducers (OMEGA PX 272) are deployed to measure the pressure fluctuations of the lower and upper sections of the dense bed. The mean distance of these pressure transducers from the distributor is 85 and 235 mm, respectively, while their respective probes are vertically spaced 50 mm. In addition, the time-averaged pressure drop along the whole bed (5–2000 mm above the distributor) is acquired through another pressure transducer (MODUS Instruments R32–100).

The tracer used for the RPT experiments is fabricated by embedding a tiny amount of a mixture of Scandium oxide and epoxy resin in a hole made in one of the biomass

Table 1. Properties of Materials Used

Material	Shape	D_p (mm)	L_p (mm)	ρ_p (kg/m^3)	ρ_b (kg/m^3)
Sand	Spherical	0.38	–	2650	1550
Biomass	Cylindrical	6.35	12.70	824	342

particles so that the size and density of the final tracer are almost identical to those of the original particle. Such a tracer could successfully mimic the motion of biomass particles while being fluidized. The tracer is then activated in the SLOWPOKE nuclear reactor of École Polytechnique up to an activity of 70 μCi. The produced isotope ^{46}Sc emits γ-rays, which are counted by 12 NaI scintillation detectors. To maximize accuracy of the RPT results, detectors are distributed on three planes such that each plane is configured 100 mm apart from the adjacent one and staggered 45° to keep the farthest distance between detectors on alternate planes. The spatial angle between two neighboring detectors in each plane is set to 90°. The horizontal distance between the column and detectors is set according to their saturation lengths measured beforehand.

A high speed data acquisition system counts the number of γ-rays detected by each detector. These counts are analyzed later to calculate the coordinates of the tracer. Details of the system calibration and the inverse reconstruction strategy for determining tracer position can be found elsewhere.[15,16] In each experiment, the location of the tracer is tracked every 10 ms for about 6 h until finally more than two million points are acquired. RPT experiments are conducted at low ($U = 0.36$ m/s) and high ($U = 0.64$ m/s) superficial gas velocities for systems containing 2, 8, and 16 wt % biomass. It is important to note that the velocity range studied is similar to that of fluidized bed gasifier but lower than the superficial gas velocity adopted typically in fluidized bed combustors (1–3 m/s).

Results and Discussion

Characterization of biomass fluidization

Analysis of the Local Pressure Drop. It is generally accepted that solids mixing in fluidized beds comprising dissimilar components is a function of the gas velocity. The local concentration of each substance, therefore, varies along the bed by changing the superficial gas velocity. These variations can be analyzed through the local time-averaged values of the signals of the pressure drop. To study the trend of mixing/segregation with gas velocity, the gradients of the local pressure drop vs. gas velocity are obtained at bottom and top of the bed. Any change in these gradients arises due to the change in the fraction of sand, biomass, and the associated voidage. The fractions pertaining to sand and voidage (gas phase) are excluded by subtracting the corresponding experimental pressure drop gradients of a bed of sand alone which is fluidized under the similar operational conditions.

The resultant parameter, that is, $\left(\left[\frac{d\Delta P}{dU}\right]_{\text{mix}} - \left[\frac{d\Delta P}{dU}\right]_{\text{sand}}\right)$ reflects changing in the fraction of biomass in the intended section with the superficial gas velocity, on the assumption that the presence of biomass does not change the void fraction of the bed of sand. Figure 1a represents variations of this parameter at the top of the bed for mixtures containing different loads of biomass. The descending trend of profiles at $U < 0.65$ m/s, indicates that the amount of biomass declines by increasing gas velocity. In other words, biomass particles which are initially accumulated on the surface of the bed at low gas velocity ($U \sim U_{ff}$) sink to the lower parts and the mixing extent of sand and biomass is enhanced along the bed. It is noteworthy that the positive effect of increasing gas velocity on the mixing of the bed components is more pronounced when the load of biomass is higher. In other words, an identical increase in gas velocity brings about a greater decrease in the content of biomass when the total quantity of biomass in the mixture is higher. The values of the investigated parameter at velocities higher than $U = 0.65$ m/s are relatively small and almost identical, regardless of the composition of the mixture. It denotes that compared to the low bubbling gas velocities, no significant change in the fraction of biomass at the top of the bed is expected when the superficial gas velocity exceeds a certain range.

Table 2. Properties of Systems Studied

Wt % of Biomass	Vol % of Biomass	Bulk Density of Sand-Biomass Mixture (10^{-3} kg/m^3)	Voidage (-)
0	0	1.49	0.42
2	6.16	1.40	0.45
4	11.82	1.36	0.44
8	21.85	1.30	0.42
16	57.72	1.17	0.40

This behavior is in total agreement with observations of Zhang et al.,[12] who studied the mixing and segregation of biomass particles in a wide range of superficial gas velocities. They reported that the biomass concentration at the top layer of the bed decreases significantly with increasing gas velocity, and at a certain velocity, it reaches a minimum, then it increases gradually. They emphasized that enhancement of mixing as a consequence of increasing gas velocity is only limited to the top part of the bed. This is the case also in the present study, as plotting $\left(\left[\frac{d\Delta P}{dU}\right]_{\text{mix}} - \left[\frac{d\Delta P}{dU}\right]_{\text{sand}}\right)$ vs. U for the bottom part of the bed brings no meaningful results.

The trend of evolution of void size distribution at the top of the bed is shown in Figure 1b. As explained in our previous work,[17] this graph was obtained by analysis of the pressure statistics. In this regard, pressure increments were initially calculated for a certain time delay (10 ms). The probability density function (PDF) of these increments was then computed and normalized to the respective standard deviation value of the pressure signal. Finally, Student's distribution (Eq. 1) was fit to the PDF to obtain two fitting parameters (α, β). It has been shown that the parameter β is related to the shape of the void size distribution around the pressure measurement probe[18]

$$\rho_s(z) = N(\alpha, \beta)[1 + \alpha z^2]^{-\beta} \tag{1}$$

As seen, the remarkable similarity between the trend of change in $\left(\left[\frac{d\Delta P}{dU}\right]_{\text{mix}} - \left[\frac{d\Delta P}{dU}\right]_{\text{sand}}\right)$ in Figure 1a and β values in Figure 1b with gas velocity signifies the existence of a linkage between the segregation pattern of biomass particles and evolution of size and shape of voidage at the top of the bed. It indicates that in systems composed of irregular particles like biomass, the local concentration of the nonconventional material governs the properties of bubbles in the bed at relatively low gas velocities.

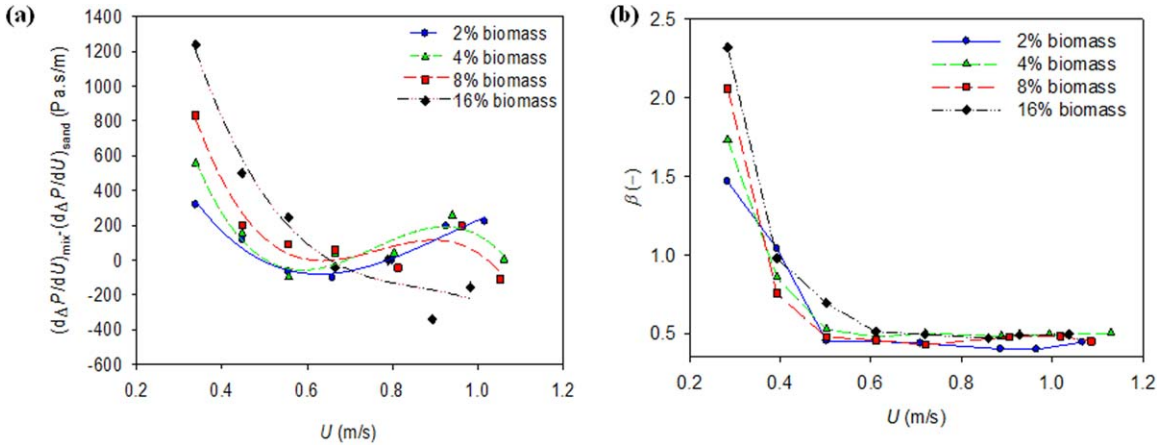

Figure 1. (a) Profile of the difference between the local pressure drop gradients of mixtures of sand and biomass and that of a similar bed composed of sand alone in bubbling regime; (b) variation of parameter β as one of the two curve fitting parameters of Student's distribution used to fit the PDF of pressure increments.

[Color figure can be viewed in the online issue, which is available at wileyonlinelibrary.com.]

Time-Averaged Concentration and Velocity Profiles of Biomass Particles. The time-averaged concentration profile of biomass particles is obtained noninvasively by the RPT method. For this purpose, the bed space is compartmentalized by means of azimuthal slices of several radial and axial cuts. The ratio of occurrence of the tracer in a specific compartment to the total number of occurrences, that is, total fraction of recorded instantaneous positions, is considered as the corresponding concentration of that compartment.

The schematic concentration profile of biomass particles in systems containing 2 and 16% wt biomass is depicted in Figure 2. Formation of a biomass-rich layer at the top, as well as a region nearly devoid of biomass at the bottom, of the bed is a common feature observed for all fluidized systems regardless of the fluidization velocity studied. Such a feature denotes the flotsam behavior of biomass particles. The expansion extent of biomass particles as a consequence of increasing the gas velocity from 0.36 to 0.64 m/s is inversely proportional to the load of biomass. In other words, the higher weight fraction of biomass is, the lower extent of biomass expansion is expected.

A very low concentration of biomass particles in the core of the bed is ascribed to the dominance of bubbles in this region. Moreover, owing to the large size of biomass particles, it is unlikely that they are lifted in the wake of bubbles. Thus, it is not surprising that the biomass concentration is substantially higher at the bed annulus compared to the bed core.

Characteristics of Biomass Circulation. The axial trajectory of the tracer consists of several ascending and descending segments representing the rising and sinking paths. Gross circulation, that is, upward movement of solids as a consequence of bubble rise and their offsetting downward flow in the dense phase is known as the main mechanism of solids mixing along the whole height of the bed. As explained by Stein et al.,[19] the cycle time, that is, the period of tracer circulation from below 30% to higher than 70% of the bed height and back, correlates with the axial mixing rate of solids. However, Stein et al. determined these boundaries based on the circulation of Geldart B particles, our studies showed that they are also appropriate to delineate the circulation path of biomass particles in the mixtures used in the present work.

The gross circulation length is defined as the maximum vertical displacement traversed by the tracer in a gross cycle. Due to the lower degree of expansion of large particles in the bed, the effective dense height (H_{eff}) decreases with increasing biomass loading and the gross cycle lengths drop

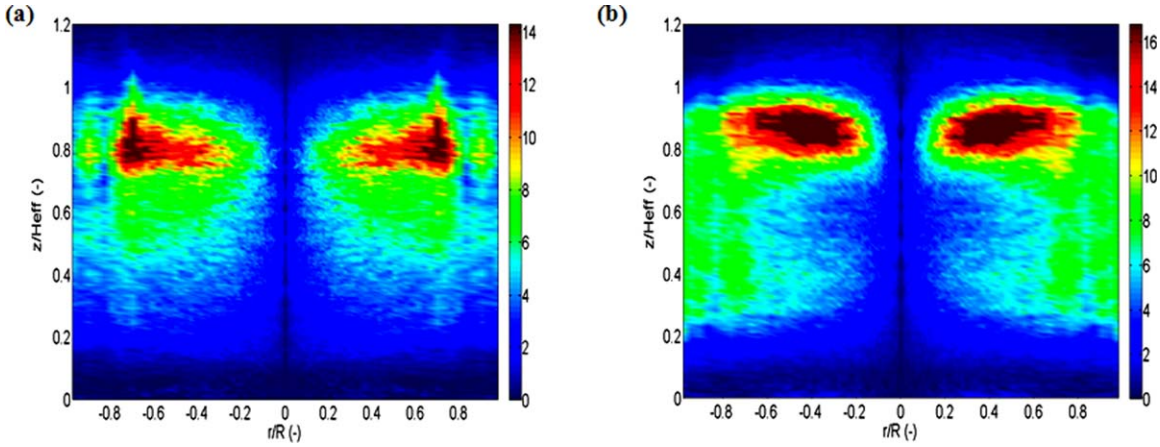

Figure 2. Time-averaged concentration (occupancy) profile of biomass particles of mixtures containing (a) 2% and (b) 16% biomass.

[Color figure can be viewed in the online issue, which is available at wileyonlinelibrary.com.]

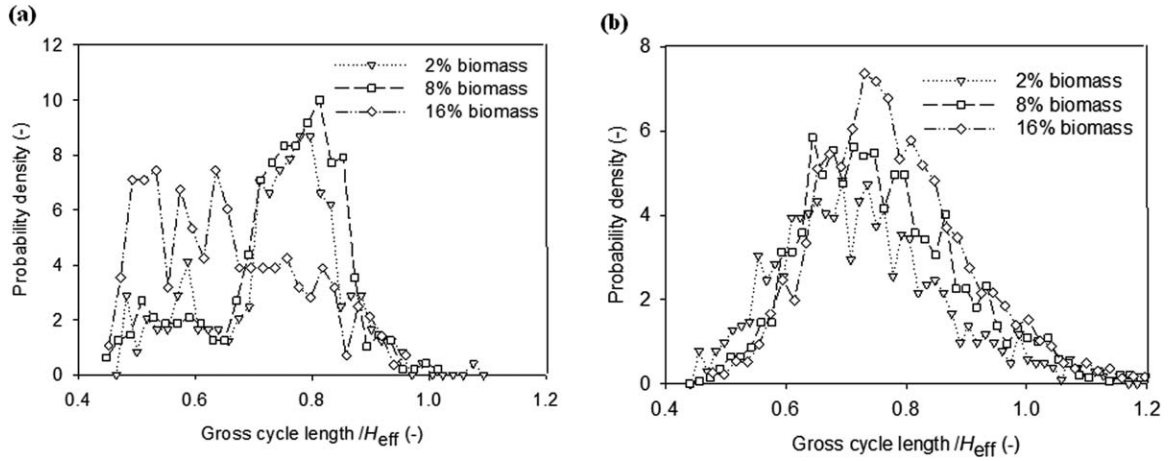

Figure 3. Probability density function of the normalized gross cycle length for systems fluidized at (a) $U = 0.36$ m/s and (b) $U = 0.64$ m/s.

proportionally. H_{eff} is defined as the height up to which 95% of all tracer occurrences took place. The probability distribution of gross circulation lengths normalized by the H_{eff} is shown in Figure 3 for systems fluidized at low and high bubbling velocities. As inferred from the relatively short lengths of the most probable gross cycles and the wide distribution of the probability density profile, fluidization of the mixture containing 16% biomass at $U = 0.36$ m/s does not result in the adequate circulation of particles in the bed. Conversely, at $U = 0.64$ m/s, the most frequent normalized gross cycle length is almost identical for all systems, whereas the corresponding frequencies rise by increasing the load of biomass. These variations signify the occurrence of more uniform cycles in the presence of larger quantities of biomass at a high enough superficial gas velocity.

The circulation pattern of an object immersed in a bubbling fluidized bed is characterized by the number of jumps occurring during its upward path as well as the maximum depth attained by the object.[2] Figure 4 shows the distribution of the number of jumps, which take place during rise of the tracer in the different systems studied. At $U = 0.36$ m/s, in spite of the shorter length of the most frequent gross cycles, a larger number of jumps occur in the case of 16% biomass. This is ascribed to the feeble bubbles inducing the jumps, which are not capable of establishing a uniform circulatory motion of biomass particles. At $U = 0.64$ m/s, however, a lower number of jumps are required to vertically lift the biomass particles for beds with higher biomass fractions. As reported previously, at high superficial gas velocities, the dense phase fraction decreases at the center of the bed with increasing biomass loadings.[17] Thus, lift of biomass particles induced by bubbles is boosted as they are subject to less resistance during their upward paths which is caused by the dense phase. The similar pattern of change in the profiles of the normalized gross cycle length and the occurrence percentage of jumps implies the pivotal role of the bubbling characteristics of the bed in governing the circulatory motion of biomass particles.

The axial loci of valleys of the tracer trajectory are analyzed to explore the extent of penetration of biomass particles within the bed. The probability density profile of the normalized maximum attainable depth (L_{max}/H_{eff}) of mixtures fluidized at $U = 0.64$ m/s is plotted in Figure 5. As defined above, H_{eff} is the height up to which 95% of all tracer occurrences take place. It was found that this limit (95%) delineates well the height of the dense bed beyond which biomass particles splash. Therefore, the zone over the dense bed height is not involved in the biomass circulation path and not shown in the graph.

As illustrated, the plots encompass two peaks. The first set of peaks signifies the downward motions disturbed by the rising bubbles impeding the sinking process. The second set

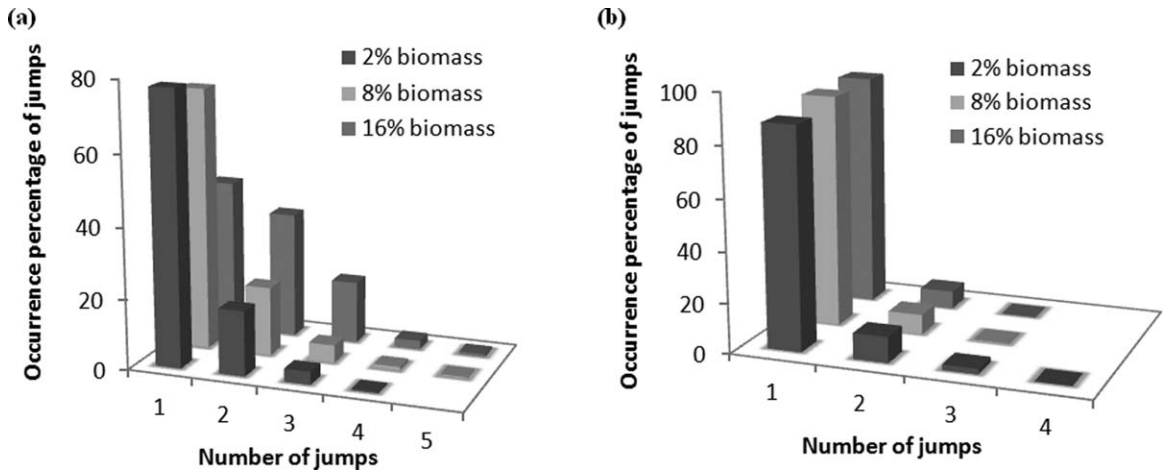

Figure 4. Occurrence percentage of jumps in gross cycles of systems fluidized at (a) $U = 0.36$ m/s and (b) $U = 0.64$ m/s.

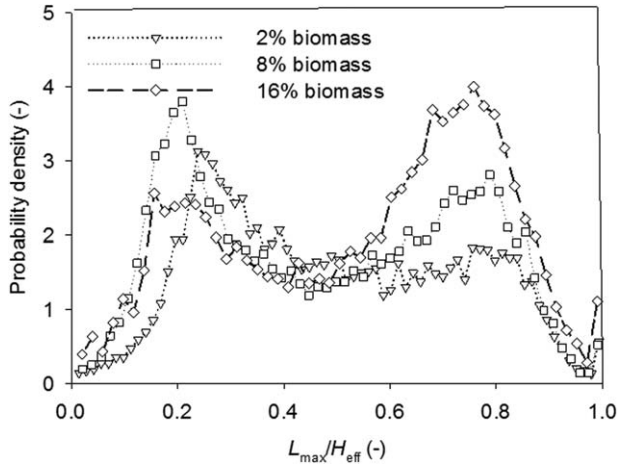

Figure 5. Probability density profile of the maximum attainable depth of biomass particles for systems fluidized at $U = 0.64$ m/s.

corresponds to the deep penetration of biomass particles achieved in the gross cycles. It is observed that the probability that biomass particles will sink to the lower level of the bed is enhanced with increasing biomass fraction in the mixture. This behavior can be explained in light of recent findings by Soria-Verdugo et al.,[3] who found that the difference between the density of a large object immersed in a bubbling fluidized bed and the bulk density of the surrounding medium governs the sinking behavior of the object. Because the bulk density of the systems studied in the present study are reduced by increasing the fraction of biomass, the net buoyant force exerted on the particles weakens proportionally. Additionally, studies of the gas distribution pattern between the dilute and dense phases show that increasing the quantity of biomass in the mixture leads to increased gas holdup and a dilution of the dense phase at the wall region.[17] Consequently, the sinking process at this zone is improved due to the higher permeability of the surrounding medium, which causes less resistance against the downward motion of the larger flotsam particles. As a result, the gross circulation of biomass particles in the bed is boosted with larger biomass loadings at high superficial gas velocities, and more successful gross cycles are observed in the bed per unit time.

Figure 6 shows the mean cycle time (the mean duration of gross cycles) and the cycle frequency (number of cycles per given period of time) in mixtures differing in the quantity of biomass fluidized at $U = 0.36$ and 0.64 m/s. As expected, increasing gas velocity reduces the mean cycling time and raises the cycle frequency. The opposite effect of biomass fraction on the cycle characteristics at low and high superficial gas velocities is clearly seen in the figure. Unlike $U = 0.36$ m/s, the mean cycle time decreases and the cycle frequency increases at $U = 0.64$ m/s with increasing the quantity of biomass. It should be noted that the mean rising and sinking velocities of biomass particles do not change meaningfully by changing the load of biomass. Therefore, the increase in the cycle frequency is solely ascribed to the increase in the number of gross cycles that come to pass during a given period of time.

The time-averaged concentration (occupancy) profiles of the biomass particles involved in gross cycles are illustrated in Figure 7 for mixtures containing 2 and 16% biomass. Increasing the number of gross cycles with the load of biomass is inferred from the higher range of the corresponding legend of Figure 7b compared to that of Figure 7a. The cross-sectional distribution of biomass particles differs also for these systems. As inferred from the position of the red spots in the figure, in the case of 2% biomass, most of the gross cycles are demarcated between the center of the lower, and the wall region of the upper, bed sections. Conversely, by raising the biomass fraction to 16%, particles start their ascent from the wall region at the bottom and move toward the center of the column as they rise. Then, particles sink from the center of the upper toward the wall region of the lower bed sections.

Mabrouk et al.[20] studied the solid holdup profile in a column 15.2 cm in diameter filled with sand up to $h/D = 2$. They found that at a given height the radial solid holdup is generally high close to the wall and declines moving toward the center of the column. In addition, it was shown that the cross-sectional averaged solid holdup increased by descending in the bed. In view of the direct correlation between the solid holdup and the local bulk density,[21] it is expected that the local bulk density will increase by going down in the bed, particularly at the wall region. As discussed earlier, the higher bulk density of the sinking medium impedes the descent of biomass particles. As a consequence, the downward pathway of the flotsam particle is dragged to the core of the bed where the particle is exposed to the less buoyant force due to the more dilute state of the bed. In light of the bubble dominancy

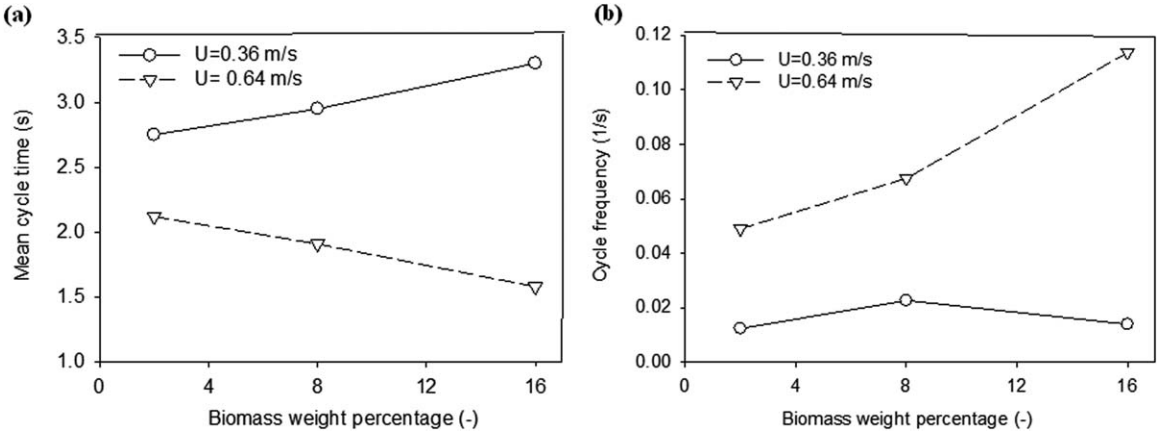

Figure 6. (a) The mean cycle time and (b) the cycle frequency of systems fluidized at $U = 0.36$ and $U = 0.64$ m/s dilute and dense phases of beds comprised of sand and biomass in a bubbling fluidization regime.

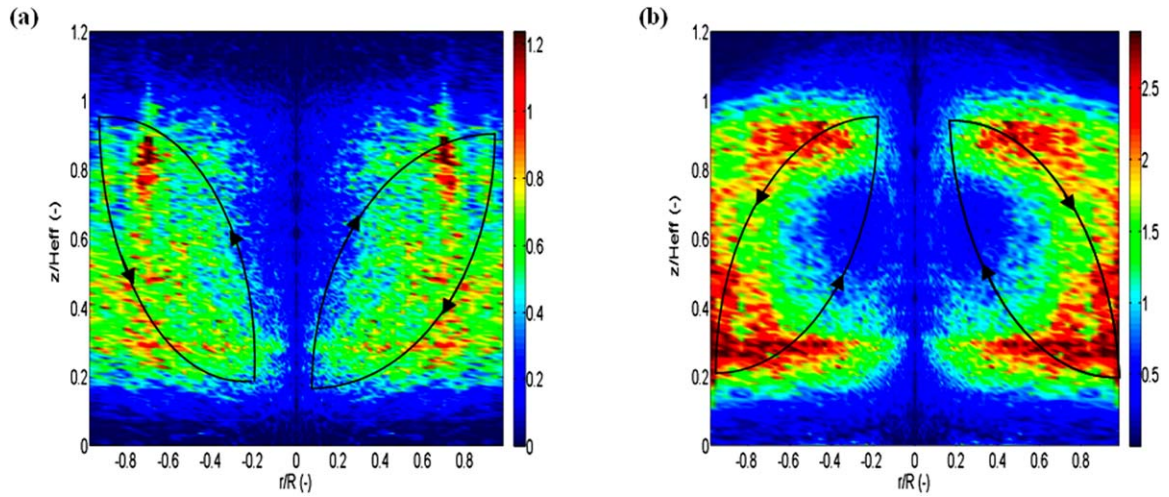

Figure 7. The time-averaged concentration (occupancy) profiles of the biomass particles involved in gross cycles at $U = 0.64$ m/s for mixtures composed of (a) 2% and (b) 16% biomass; the most probable pathway of the biomass gross cycle has been illustrated by the black curves.

[Color figure can be viewed in the online issue, which is available at wileyonlinelibrary.com.]

at the core of the bed, however, biomass particles are prone to be involved in a rising process before a thorough sinking thus, reducing overall mixing. When the biomass load is increased, the bulk mixture density decreases and it has been shown that, when the biomass fraction increased from 2 to 16%, the mean bubble size became smaller and the dense phase fraction at the wall region fell remarkably.[17] Hence, the sinking process could be carried out in the annular region of the bed and flotsam particles penetrate more effectively into the lowermost sections without being disturbed by the passage of large bubbles. In view of these phenomena, the most probable pathway of biomass gross cycles has been plotted in Figure 7.

It is worth pointing out that these differences matter from the practical point of view for considering an adequate location for the feeding locations. In other words, the optimal feeding point can depend on the composition of the bed inventory. Radmanesh et al.[5] showed that the feeding location could significantly affect distribution of gas products in the bed. In bottom feeding, the product gases from the pyrolysis step enter directly into the region of the bed where the concentration of oxygen is high. As a result, light gases, such as H_2 and CO, as well as tar, are prone to combustion in the bed. Conversely, in top feeding, the gas product from the pyrolysis step enters in a region that has already become depleted of oxygen, mainly through the char combustion in the bed. Consequently, concentrations of H_2 and CO are higher and cracking and combustion of tar is less prone.

In view of the influence of the composition of the bed inventory on the locus of the most probable circulation pathway of the biomass particles, it is inferred that the inward ascent (from the wall toward the central region) and the outward descent (from the center toward the wall of the bed) are the favored paths for occurrence of a higher degree of the axial mixing. This fact is a matter of importance in designing the feeding points of biomass combustors/gasifiers. In addition, the effectiveness of top or bottom feeding can be changed by changing the composition of the mixture fluidized in the bed. For instance, in the case of bottom feeding for the mixture composed of 16% biomass, particles are prone to being drawn into the rise path of the gross cycles as soon as being fed into the bed, whereas for the mixture containing 2% biomass, particles can rest longer in the lower part of the bed as the loci of gross cycles are far from the wall proximity in this region. Thus, it is expected that in the case of bottom feeding, contact of the pyrolysis products and oxygen takes place more effectively when the load of biomass is lower. Conversely, as biomass particles are subject to descend in the wall region when the load of biomass in the bed is high, it is more likely that they will react effectively with the interstitial oxygen of the dense phase, thereby improving the reactor performance.

Quantification and modeling the axial distribution of the volume fraction of biomass

Distribution of bed components along the bed is usually quantified through obtaining the axial profile of the volume fraction of jetsam or flotsam particles. In the present study, the volume fraction of biomass (X_B) is obtained by postprocessing of the RPT data through the virtual slicing of the bed and computing the ratio of occurrence of the tracer in a specific slice to the total number of occurrences, that is, the total number of recorded instantaneous positions. These values are then related to the volume fractions of biomass in each slice knowing the quantities of sand and biomass mixed initially and the respective densities.

To compare the degree of uniformity of biomass distribution in mixtures differing in biomass fractions, X_B is normalized to the total volume fraction of biomass in the bed ($X_{B,total}$). As depicted in Figure 8, increasing gas velocity gives rise to a shift in the normalized X_B values, particularly at the middle height of the bed, to the dashed line indicating a perfectly mixed state. This improvement in the mixing state is more pronounced for systems containing 8 and 16% biomass, signifying the positive effect of the higher load of biomass particles on their even distribution along the bed.

To model the axial distribution of biomass, the principles of the Gibilaro and Rowe (G-R) model[22] are applied, however, unlike the G-R and other common models in which the jetsam profile is studied, the concentration profile of the flotsam component is described in the current model.

As the bed is composed of dense and dilute phases, it has been assumed that the dilute phase is devoid of biomass

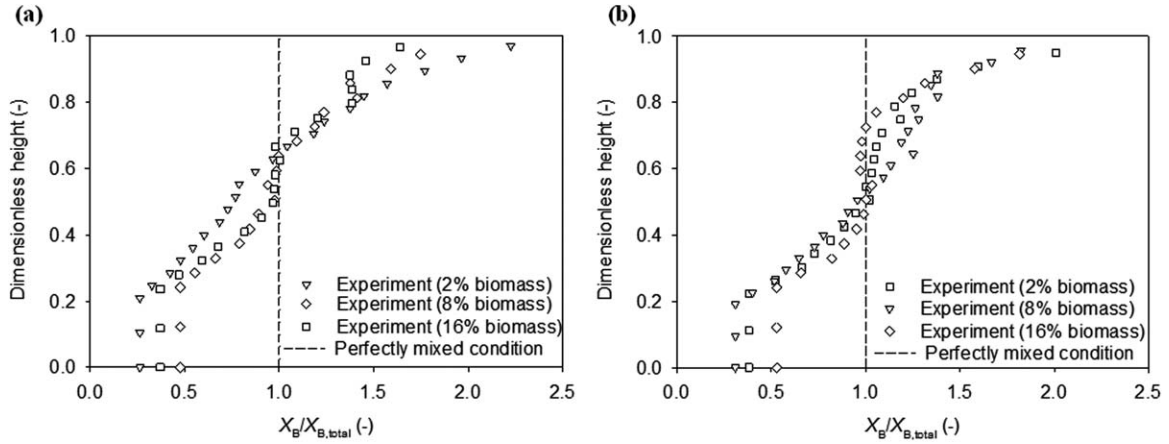

Figure 8. The experimental normalized volume fraction of biomass ($X_B/X_{B,total}$) vs. the dimensionless height at (a) $U = 0.36$ m/s and (b) $U = 0.64$ m/s.

particles because of their extreme size. The rise of biomass particles mainly occurs due to the intermittent jerks produced by a drift mechanism as a consequence of successive bubble passes. In addition, as bubbles travel preferentially in the central region of the bed, a large scale circulation is also felt by the flotsam particles. Jetsam particles, however, rise in the dilute phase and descend in the dense phase. Therefore, they can be exchanged between dilute and bubble phases. As reported by other researchers,[8,23,24] contribution of the jetsam axial mixing and segregation propensity to the material balances for solids mixing is negligible under the conditions of biomass fluidization, thus they have not been considered in the proposed model. Figure 9 depicts a diagram of a horizontal layer of the bed of dZ thickness to which the mass balances of both phases have been applied. The mathematical expression of each term is as follows.

Fluidization medium (sand in our experimental systems) rises along the bed in the wake of bubbles and sinks in the dense (emulsion) phase. Thus, the flow of rising sand, that is, $\psi_F^b(m^3/s)$, is formulated as below

$$\psi_F^b = U_b \delta_b F_w (1-\varepsilon_F) A \tag{2}$$

where ε_F is the voidage of the emulsion phase of a bed containing sand only. It has been calculated by the Cui et al. correlation[25] taking into consideration the effect of gas velocity (Eq. 3)

$$\varepsilon_F = \varepsilon_{mf} + 0.2 - 0.059 \exp\left[-\frac{(U-U_{ib})}{0.429}\right] \tag{3}$$

The volume fraction occupied by bubbles has been calculated using Eq. 4. Y indicates the degree of deviation of the bed from the "two-phase theory". Because sand is the dominant component in the investigated mixtures in terms of weight and volume, $Y = 0.7$ is chosen as a typical assumption for the Geldart B particles. As reported in another work,[17] the presence of biomass particles could delay the onset of bubbling compared to the bed of sand alone. Thus, it is reasonable to use the initial bubbling velocity (U_{ib}) instead of U_{mf} of sand in order to evaluate the excess gas velocity

$$\delta_b = \frac{Y(U-U_{ib})}{U_b} \tag{4}$$

On the basis of the analysis of the biomass rise velocity realized through postprocessing of the RPT data, it was found that the average rise velocity of biomass particles is around 0.2 times the average bubble rise velocity (Figure 10), consistent with the findings of Soria-Verdugo et al.[2] As discussed below, bubble size and velocity are calculated by using Darton et al.[26] and Davidson and Harrison[27] equations (Eqs. 9 and 10), respectively. To calculate the mean bubble rise velocity, the latter equation is integrated and averaged along the bed height. Thus, the ratio of biomass to bubble velocity (0.2) is a height-averaged value.

In view of the rise of biomass particles in the emulsion phase, the rising flow of biomass, that is, $\psi_B^e(m^3/s)$ is obtained by Eq. 5

$$\psi_B^e = 0.2 U_b (1-\delta_b)(1-\varepsilon_e) X_{B_e} A \tag{5}$$

ε_e is the voidage of the emulsion phase in a mixture containing fluidization medium and biomass particles and, as proposed by Bilbao et al.,[24] it can be calculated using Eq. 6 based on the fact that the fluidization medium occupies the voidage between biomass particles

$$\varepsilon_e = 1 - \frac{1-s_B}{1-X_{F_e}} \tag{6}$$

Equation 6 is valid when $X_{B_e} > \frac{1-s_B}{1-s_F}$. For lower values of X_{B_e}, it is assumed that the voidage of the mixture emulsion phase (ε_e) equals to the voidage of a bed of fluidization medium alone (ε_F).

The exchange rate of the fluidization medium between bubble and emulsion phases per unit of bed height can be described by Eq. 7

$$q = K_w \delta_b (1-\varepsilon_F) A \tag{7}$$

Assuming that the exchange coefficient between the constitutive phases (K_w) is not affected by the biomass particles, the correlation introduced by Hoffmann et al.[28] (Eq. 8) is chosen to calculate K_w from properties of the bed as pointed out by Radmanesh et al.[5]

$$K_W = \frac{0.081}{2 s_{mf} d_b} \tag{8}$$

One of the common assumptions in modeling binary mixtures is that the bubbling characteristics of the system are those of a bed of pure fluidization medium. However, it was

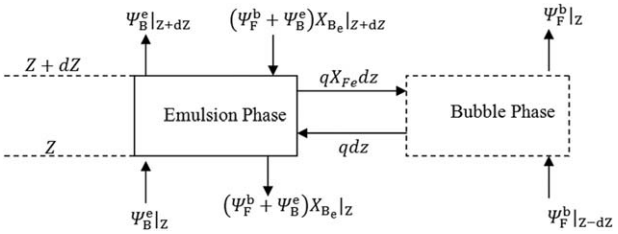

Figure 9. Diagram of the model.

revealed that the presence of biomass particles led to the breakage of bubbles.[17] From a holistic point of view, the mean bubble size and velocity in all systems could be fairly predicted by correlations of Darton et al.[26] (Eq. 9), and Davidson and Harison[27] (Eq. 10), respectively, regardless of the biomass fraction. It should be noted that other correlations, such as those developed by Choi et al.,[29] Cai et al.,[30] and Horio and Nonaka,[31] predict smaller values than the bubble size measured experimentally and their use in the model leads to predictions not in agreement with the present data

$$d_b = 0.54 g^{-0.2} (U - U_{ib})^{0.4} (Z + 4A_c^{0.5})^{0.8} \quad (9)$$

$$U_b = 0.711\sqrt{g d_b} + (U - U_{ib}) \quad (10)$$

A mass balance on a slice of the bed for both bubble and emulsion phases can be summarized as follows

$$\frac{dX_{B_e}}{dz} = \frac{qX_{B_e}}{\psi_F^b + \psi_B^e} \text{ B.C. } X_{B_e} = X_{B_{e0}}\ Z = 0 \quad (11)$$

The axial volume fraction of biomass (X_B) is derived from X_{B_e} values through the following equation

$$X_B = \frac{(1-\delta_b)(1-s_e)X_{B_e}}{(1-\delta_b)(1-s_e) + F_W \delta_b (1-s_F)} \quad (12)$$

A computer program was developed to fit the experimental data with the above equations. To do so, the bed was discretized into successive layers. Equation 11 was then converted into linear equations using a finite difference scheme and solved numerically for each layer. The boundary value ($X_{B_{e0}}$) was the only adjustable parameter. It should be noted that as exhibited in Figure 2, the lowermost 50 mm of the bed in all studied cases is almost devoid of biomass and

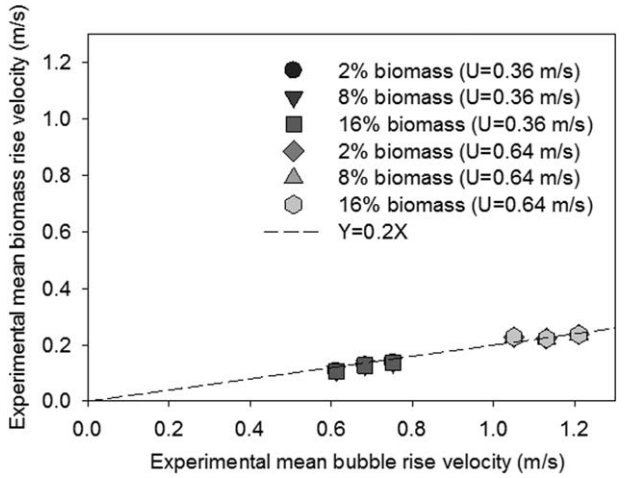

Figure 10. Mean rising velocities of biomass particles along the bed compared with the mean velocity of bubbles.

this layer is not involved in the circulatory motion of biomass particles presumably because of the ineffective bubbling conditions in this zone. Hence, the volume fraction of biomass in this part was considered as the boundary condition of the model.

Figure 11 shows the experimental profile of biomass concentration along the bed compared to the model proposed at two different fluidization velocities. In general, the model proposed could satisfactorily estimate the experimental data, particularly when the load of biomass is low. By increasing the weight fraction of biomass, however, the fitting quality slightly declines mainly because of the considerable deviation of the actual bubble size from what is predicted by the correlation of Darton et al. Indeed, it is expected that the prediction capacity of the model would improve significantly if the effect of biomass on the bubbling behavior of systems could be taken into account more accurately. To keep the proposed model free of any adjustable parameter, it is reasonable to relate $X_{B_{e0}}$ to the fluidization velocity (U) and the weight fraction of biomass in the mixture (x_{Bm}). Applying a multivariable data fitting reveals that $X_{B_{e0}}$ is related to x_{Bm} and U as below

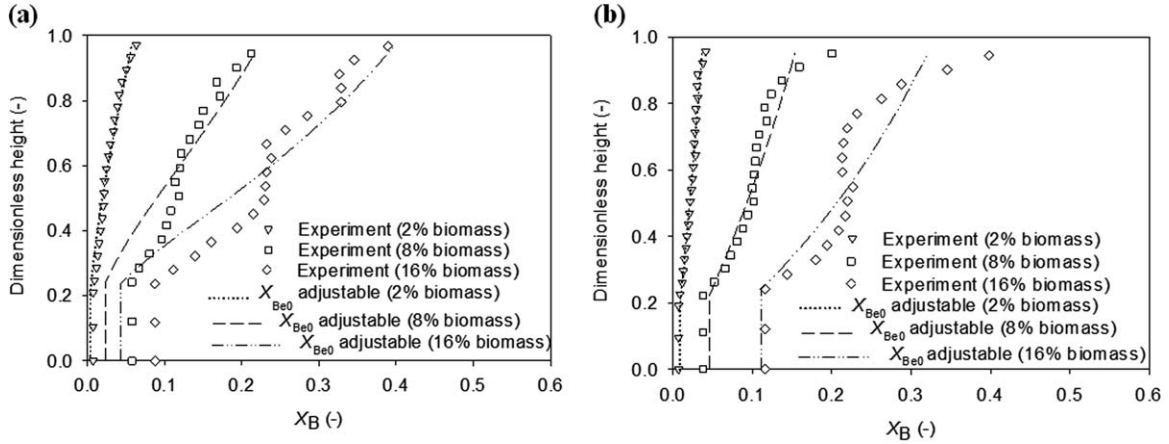

Figure 11. The experimental and modeled volume fraction of biomass (X_B) vs. the dimensionless height of the mixtures containing 2, 8, and 16% biomass fluidized at (a) $U = 0.36$ m/s and (b) $U = 0.64$ m/s; $X_{B_{e0}}$ is the single adjustable parameter in the model used determined by data fitting.

Table 3. Comparing the Values of $X_{B_{e0}}$ Obtained from the Fitting of Experimental Data and Eq. 13 ($k = 2$)

Load of Biomass (%)	Gas Velocity (m/s)	$X_{B_{e0}}$ (Fitting)	$X_{B_{e0}}$ (Eq. 13)
2	0.36	0.0041	0.0036
	0.64	0.0089	0.009
8	0.36	0.0237	0.0188
	0.64	0.0459	0.0473
16	0.36	0.0431	0.0433
	0.64	0.1119	0.1086

$$X_{B_{e0}} = k x_{Bm}{}^{1.2} U^{1.6} \quad (13)$$

Since Eq. 13 has been obtained for the lowermost part of the bed, adjacent to the distributor, dependency of the volume fraction of biomass on superficial gas velocity can be linked to the parameters governing the multiple gas inlet jets. It has been shown that the minimum moving zone diameter (d_m) around the jetting zone is correlated to $U^{1.5}$.[32] As indicated by Agarwal et al.,[33] this zone contains slow moving emulsion particles entraining into the jets and its demarcation is pivotal in determining the particle circulation volume in the region above the distributor base and below the jet penetration height. By enlarging this zone as a consequence of increasing gas velocity, the likelihood of biomass penetration from the upper layers to the distributor region is enhanced.

Table 3 compares the values of the $X_{B_{e0}}$ obtained from the fitting of experimental data and Eq. 13. Furthermore, experimental data and a model in which Eq. 13 is considered as the boundary condition have been compared in Figure 12. As seen, use of Eq. 13 in the suggested model for estimating $X_{B_{e0}}$ brings about the acceptable prediction of the biomass distribution profile along the bed.

Carrying out sensitivity analysis reveals that the sensitivity of the profile of biomass volume fraction to the load of biomass increases by increasing the superficial gas velocity. In other words, at high gas velocities, a slight change in the load of biomass could significantly impact biomass distribution along the bed. It is consistent with the above discussion considering the improvement in the circulation of large particles by increasing their fraction in the bed at $U = 0.64$ m/s.

To verify the suitability of the proposed model to predict the distribution of biomass in other experimental systems, it was applied to the experimental data of Bilbao et al.,[24] who obtained the axial volume fraction profile of straw particles mixed with sand in a small fluidization column (i.d. = 8 cm). To extract the volume fraction of sand along the bed, Bilbao et al. followed the "freezing bed" technique, that is, they suddenly stopped the air flow and extracted 1-cm thick bed layers. It should be noted that this method does not allow for considering the real voidage of the bed under fluidization conditions; therefore, the reported values may not be representative of the real axial distribution of the particles.

Considering the different properties of straw from those of the biomass particles used in our experiments, a sensitivity analysis was performed with respect to the ratio of the average rise velocity of biomass particles to that of bubbles in the bed $\left(\frac{\bar{U}_{bm}}{U_b}\right)$. As shown in Figure 13, $\frac{\bar{U}_{bm}}{U_b} = 0.3$ is the optimal ratio resulting in the predicted values representing the experimental data. Increase in $\frac{\bar{U}_{bm}}{U_b}$, respecting the ratio used in the present study (0.2), is justifiable in light of the smaller size and the lower density of the straw particles compared with the large wood pieces fluidized with sand.

As demonstrated in Figures 14 and 15, the error between the experimental and the corresponding model values for systems differing in composition and fluidization velocity decreases slightly when $\frac{\bar{U}_{bm}}{U_b}$ changes from 0.2 to 0.3.

The above discussion indicates that further experimental work is required to improve the developed model (with no adjustable parameter) in order to make it fully applicable to the fluidized beds involving various types of inert and biomass particles in terms of size, density, and shape.

Conclusions

The distribution of large biomass particles along a bubbling fluidized bed was studied experimentally through analysis of the local pressure fluctuations and inference of the biomass particle circulation patterns. The axial particle dispersion in the bed was explored by tracing the trajectory of an active tracer in mixtures containing different weight fractions of biomass. The occurrence of segregation in the bed was qualitatively perceived through the local time-averaged pressure drops as well as the time-averaged occupancy profile obtained by the RPT technique. Increasing the biomass fraction at $U = 0.36$ m/s leads to the imperfect circulation and severe segregation of biomass particles. However, at $U = 0.64$ m/s higher quantities of biomass in the bed

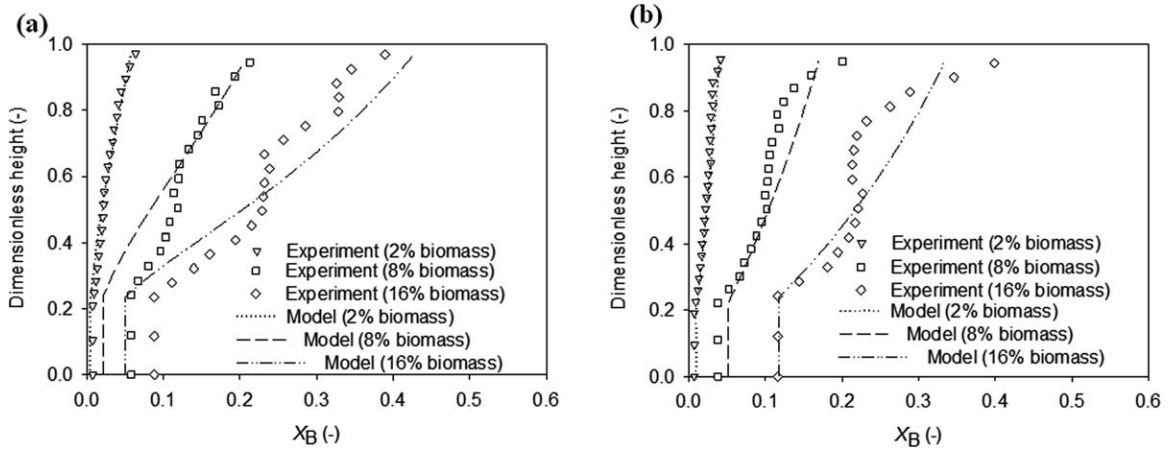

Figure 12. The experimental and modeled volume fraction of biomass (X_B) vs. the dimensionless height of the mixtures containing 2, 8, and 16% biomass fluidized at (a) $U = 0.36$ m/s and (b) $U = 0.64$ m/s when Eq. 13 is used to estimate $X_{B_{e0}}$.

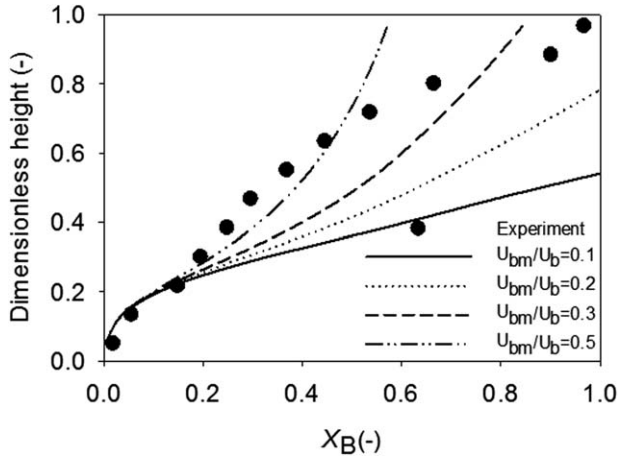

Figure 13. Sensitivity of the model proposed with respect to $\frac{U_{bm}}{U_b}$, as applied to the experimental data of Bilbao et al.,[24] (fluidization of straw-sand mixtures at $U = 0.14$ m/s, ($x_{straw} = 0.08$, $d_{sand} = 158$ μm, $d_{straw} = 794$ μm, $\rho_{sand} = 2000$ kg/m^3, $\rho_{straw} = 350$ kg/m^3).

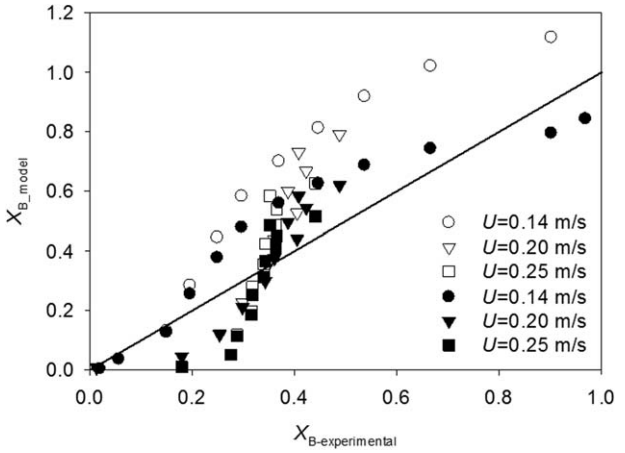

Figure 15. The values predicted by the proposed model when $\frac{U_{bm}}{U_b} = 0.2$ (white symbols) and $\frac{U_{bm}}{U_b} = 0.3$ (black symbols) vs. the corresponding experimental data reported by Bilbao et al.[24] ($x_{sand} = 0.08$, $d_{sand} = 158$ μm, $d_{straw} = 794$ μm, $\rho_{sand} = 2000$ kg/m^3, $\rho_{straw} = 350$ kg/m^3).

improve the sinking process of biomass and bring about a more uniform distribution of biomass throughout the bed. Considering the enhanced mixing state and the loci of the most probable pathway of biomass circulation, it is expected that the impact of the feeding location (top or bottom feeding) on the distribution of gas products in the bed diminishes by increasing the biomass fraction under vigorous bubbling conditions.

The parameters relating terms of the G-R model to the operating conditions were improved on the basis of the experimental findings describing the motion of the flotsam particle and the characteristics of bubbling. Analysis of the experimental data acquired by the RPT technique revealed that the averaged rise velocity of biomass particles is around 0.2 times the bubble velocity in the bed regardless of the biomass load or fluidization velocity. A model has been proposed that could successfully predict the volume fraction of biomass along the bed. It was shown that the biomass volume fraction in the grid-zone region of the fluidized bed is correlated to the superficial gas velocity and the load of biomass.

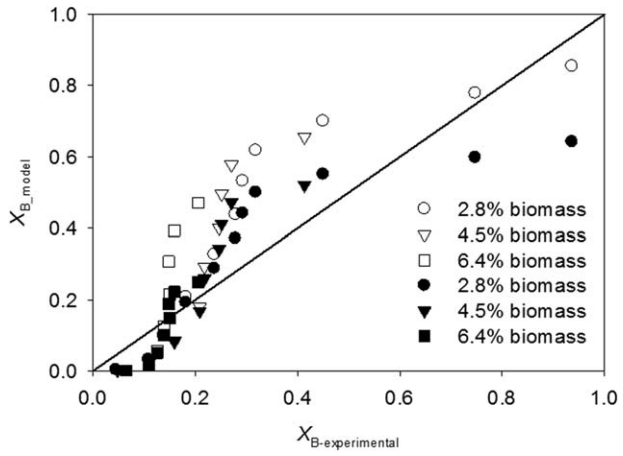

Figure 14. The values predicted by the proposed model when $\frac{U_{bm}}{U_b} = 0.2$ (white symbols) and $\frac{U_{bm}}{U_b} = 0.3$ (black symbols) vs. the corresponding experimental data reported by Bilbao et al.[24] ($U = 0.17$ m/s, $d_{sand} = 158$ μm, $d_{straw} = 1265$ μm, $\rho_{sand} = 2000$ kg/m^3, $\rho_{straw} = 350$ kg/m^3).

Acknowledgment

This work was funded by the Natural Science and Engineering Research Council (NSERC) and TOTAL American Services, Inc. industrial chair.

Notation

A = cross-sectional area of the bed, m^2
A_C = catchment area of a hole in the distributor, m^2
H_{eff} = effective height of the bed up to which 95% of all tracer occurrences takes place, m
F_w = ratio of bubble wake volume to bubble volume, 0.185
K_W = exchange coefficient between the dilute and dense phases, s^{-1}
L_{max} = maximum attainable depth of biomass particles
$N[\alpha,\beta]$ = normalization factors of the student's distributions,
U = superficial gas velocity, ms^{-1}
U_b = bubble rise velocity, ms^{-1}
U_{ib} = initial bubbling velocity, ms^{-1}
X_B = volume fraction of biomass in a specific layer
$X_{B,total}$ = total volume fraction of biomass along the bed
X_{B_e} = volume fraction of biomass in the emulsion phase of a specific layer
$X_{B_{e0}}$ = volume fraction of biomass in the emulsion phase at $Z = 0$
X_{F_e} = volume fraction of fluidization medium in the emulsion phase of a specific layer
Y = deviation factor from two-phase theory of fluidization
Z = height above the distributor plate, m
d_b = bubble diameter, m
d_m = minimum moving zone diameter, m
d_{sand} = mean size of sand particles, m
d_{straw} = mean size of straw particles, m
q = bubble-emulsion exchange coefficient, m^2 s^{-1}
x_{Bm} = weight fraction of biomass in the mixture
x_{straw} = weight fraction of straw in the mixture
z = generic random variable
ψ_B^e = volumetric flow rate of biomass in the emulsion phase, m^3 s^{-1}
ψ_F^b = volumetric flow rate of fluidization medium in the bubble phase, m^{3}s^{-1}
α,β = curve-fitting parameters for student's distribution
δ_b = volume fraction of bubbles in bed
ε_e = void fraction of emulsion phase in a biomass-fluidization medium mixture

ε_B = void fraction of a bed of biomass alone
ε_F = void fraction of a bed of fluidization medium alone
ε_{mf} = ε_F at minimum fluidization conditions
ρ_{sand} = density of sand, kg m^{-3}
ρ_{straw} = density of straw, kg m^{-3}

Literature Cited

1. Cui H, Grace JR. Fluidization of biomass particles: a review of experimental multiphase flow aspects. *Chem Eng Sci*. 2007;62(Compendex):45–55.
2. Soria-Verdugo A, Garcia-Gutierrez LM, Sanchez-Delgado S, Ruiz-Rivas U. Circulation of an object immersed in a bubbling fluidized bed. *Chem Eng Sci*. 2011;66(1):78–87.
3. Soria-Verdugo A, Garcia-Gutierrez LM, Garcia-Hernando N, Ruiz-Rivas U. Buoyancy effects on objects moving in a bubbling fluidized bed. *Chem Eng Sci*. 2011;66(12):2833–2841.
4. Rees AC, Davidson JF, Dennis JS, Hayhurst AN. The rise of a buoyant sphere in a gas-fluidized bed. *Chem Eng Sci*. 2005;60(4):1143–1153.
5. Radmanesh R, Chaouki J, Guy C. Biomass gasification in a bubbling fluidized bed reactor: experiments and modeling. *AIChE J*. 2006; 52(12):4258–4272.
6. Rios GM, Dang Tran K, Masson H. Free object motion in a gas fluidized bed. *Chem Eng Commun*. 1986;47(4–6):247–272.
7. Lim KS, Agarwal PK. Circulatory motion of a large and lighter sphere in a bubbling fluidized bed of smaller and heavier particles. *Chem Eng Sci*. 1994;49(3):421–424.
8. Pallares D, Johnsson H. A novel technique for particle tracking in cold 2-dimensional fluidized beds - simulating fuel dispersion. *Chem Eng Sci*. 2006;61(8):2710–2720.
9. Larachi F, Cassanello M, Marie M, Chaouki J, Guy C. Solids circulation pattern in 3-phase fluidized-beds containing binary-mixtures of particles as inferred from RPT *Chem Eng Res Des*. 1995;73(A3): 263–268.
10. Cassanello M, Larachi F, Guy C, Chaouki J. Solids mixing in gas-liquid-solid fluidized beds: experiments and modelling. *Chem Eng Sci*. 1996;51(10):2011–2020.
11. Upadhyay RK, Roy S. Investigatin of hydrodynamics of binary fluidized beds via radioactive particle tracking and dual-source densitometry. *Can J Chem Eng*. 2010;88(4):601–610.
12. Zhang Y, Jin B, Zhong W. Experimental investigation on mixing and segregation behavior of biomass particle in fluidized bed. *Chem Eng Process*. 2009;48(3):745–754.
13. Zhang Y, Jin B, Zhong W. Fluidization, mixing and segregation of a biomass-sand mixture in a fluidized bed. *Int J Chem React Eng*. 2008;6:1–29.
14. Geldart D. Types of gas fluidization. *Powder Technol*. 1973;7(5): 285–292.
15. Larachi F, Chaouki J, Kennedy G. 3-D Mapping of solids flow-fields in multiphase reactors with RPT *AIChE J*. 1995;41(2):439–443.
16. Larachi F, Kennedy G, Chaouki J. A gamma-ray detection system for 3-D particle tracking in multiphase reactors. *Nucl Instrum Methods Phys Res A*. 1994;338(2–3):568–576.
17. Fotovat F, Chaouki J, Bergthorson J. The effect of biomass particles on the gas distribution and dilute phase characteristics of sand-biomass mixtures fluidized in bubbling regime. *Chem Eng Sci*. 2013; 102(0):129–138.
18. Bai B, Gheorghiu S, van Ommen JR, Nijenhuis J, Coppens MO. Characterization of the void size distribution in fluidized beds using statistics of pressure fluctuations. *Powder Technol*. 2005;160(2):81–92.
19. Stein M, Martin TW, Seville JPK, McNeil PA, Parker DJ. Positron emission particle tracking: particle velocities in gas fluidised beds, mixers and other applications. In: Jamal C, Faïcal L, Milorad PD, editors. Non-Invasive Monitoring of Multiphase Flows, Chapter 10. Amsterdam: Elsevier Science B.V., 1997:309–333.
20. Mabrouk R, Radmanesh R, Chaouki J, Guy C. Scale Effects on Fluidized Bed Hydrodynamics. *Int J Chem React Eng*. 2005;3(1):1–11.
21. Escudero D, Heindel TJ. Bed height and material density effects on fluidized bed hydrodynamics. *Chem Eng Sci*. 2011;66(16):3648–3655.
22. Gibilaro LG, Rowe PN. A model for a segregating gas fluidized bed. *Chem Eng Sci*. 1974;29(6):1403–1412.
23. Nienow AW, Chiba T. Fluidization of dissimilar materials. *Fluidization*, 1985:357–382.
24. Bilbao R, Lezaun J, Menendez M, Abanades JC. Model of mixing segregation for straw/sand mixtures in fluidized beds. *Powder Technol*. 1988;56(3):149–155.
25. Cui HP, Mostoufi N, Chaouki J. Characterization of dynamic gas-solid distribution in fluidized beds. *Chem Eng J*. 2000;79(2):133–143.
26. Darton RC, LaNauze RD, Davidson JF, Harrison D. Bubble growth due to coalescence in fluidised beds. *Trans Inst Chem Eng*. 1977; 55(4):274–280.
27. Davidson JF, Harrison, D. Fluidised Particles. Cambridge: Cambridge University Press, 1963.
28. Hoffmann AC, Janssen L, Prins J. Particle segregation in fluidized binary-mixtures. *Chem Eng Sci*. 1993;48(9):1583–1592.
29. Choi JH, Jae ES, Sang Done K. Bubble size and frequency in gas fluidized beds. *J Chem Eng Jpn*. 1988;21:171–178.
30. Cai P, Schiavetti M, Demichele G, Grazzini GC, Miccio M. Quantitative estimation of bubble-size in PFBC. *Powder Technol*. 1994; 80(2):99–109.
31. Horio M, Nonaka A. A generalized bubble diameter correlation for gas-solid fluidized beds. *AICHE J*. 1987;33(11):1865–1872.
32. Horio M, Kiyota H, Muchi I. Particle movement on a perforated plate distributor of fluidized bed. *J Chem Eng Jpn*. 1980;13(2):137–142.
33. Agarwal G, Lattimer B, Ekkad S, Vandsburger U. Influence of multiple gas inlet jets on fluidized bed hydrodynamics using particle image velocimetry and digital image analysis. *Powder Technol*. 2011;214(1):122–134.

Manuscript received Jun. 24, 2013, and revision received Nov. 18, 2013.